ARTICLE

Electrochemical Performance and Capacity Fading Mechanism of $LiFePO_4$ at Different pH Aqueous Electrolyte Solutions

Yuan Yin[a,b], Yue-hua Wen[b*], Yong-lai Lu[a*], Jie Cheng[b], Gao-ping Cao[b], Yu-sheng Yang[a,b]

a. College of Materials Science and Engineering, Beijing University of Chemical Technology, Beijing 100029, China

b. Research Institute of Chemical Defence, Beijing 100191, China

(Dated: Received on February 8, 2015; Accepted on April 14, 2015)

The electrochemical stability of $LiFePO_4$ in a Li^+-containing aqueous electrolyte solution is critically dependent on the pH value of the aqueous solution. It shows a considerable decay in capacity of $LiFePO_4$ upon cycling when the pH value is increased to 11. The mechanism responsible for the capacity fading is extensively investigated by means of cyclic voltammogram, ac impedance, charge/discharge, *ex situ* X-ray diffraction, and chemical analysis. $LiFePO_4$ is relatively electrochemically stable in $LiNO_3$ aqueous solution with pH=7. But the electrochemical performance of $LiFePO_4$ in aqueous electrolyte is inferior to that in organic electrolyte. It is attributed to the loss of Li and the Fe, P dissolution during prolonged charge-discharge in aqueous medium. A precipitate is formed on the surface of $LiFePO_4$ electrodes. It results in the change of crystalline structure, a large electrode polarization, and capacity fading.

Key words: Olivine $LiFePO_4$, Aqueous electrolyte, Electrochemical property, Capacity fade, Mechanism

I. INTRODUCTION

Lithium iron phosphate ($LiFePO_4$) with an ordered olivine structure has been proposed to be a potential candidate as cathode in non-aqueous electrolyte lithium batteries and has been widely studied and used in non-aqueous secondary batteries [1–5]. In contrast, the electrochemistry of this transition metal oxide in aqueous electrolyte systems attracted far less attention. There were several investigations of the possibility of the use of lithium reactant electrodes in aqueous electrolytes during the 1990s [6–9]. This approach has several obvious potential advantages over organic solvent electrolyte lithium batteries, including greater safety and low cost. Various aqueous lithium-ion batteries such as $LiV_3O_8/LiMn_2O_4$ [10, 11], $LiV_3O_8/LiCoO_2$ [11], $LiTi_2(PO_4)_3/LiFePO_4$ [12] and $LiTi_2(PO_4)_3/LiMn_2O_4$ [12–14] systems have also been reported. However, most of these systems show poor cycling stability, especially at a low current rate. The cycling number of charge-discharge is generally less than 200 cycles. Studies on the mechanism of capacity fading during cycling in aqueous lithium-ion batteries mostly focus on the dissolution of electrode materials and side reactions of hydrogen or oxygen evolution. In addition, the electrochemical stability of $LiMn_2O_4$, $LiNi_{1/3}Co_{1/3}Mn_{1/3}O_2$ and $LiCoO_2$ are critically dependent on the pH value of aqueous electrolyte. It has been reported that prolonged exposure of $LiFePO_4$ to oxygen or water resulted in Li loss and increase of Fe (III) content [15–17], particularly with alkaline aqueous solutions. Porcher *et al.* investigated the stability of $LiFePO_4$ in water, and reported that if experimental conditions such as immersion time, pH, and $LiFePO_4$ concentration were set to optimal values, the formation of a Li_3PO_4 passive layer did not alter significantly the electrochemical behavior of $LiFePO_4$ [15]. Lee *et al.* investigated the correlation between Li and Fe ion dissolution behavior as functions of pH and surface chemistry of $LiFePO_4$ nanoparticles and the electrochemical properties of $LiFePO_4$ positive electrodes in organic electrolyte [18]. It was found that the dissolution of Li and Fe ions in aqueous processing yielded a depleted powder that had a lower rate capability for $LiFePO_4$ cathodes. However, Huang *et al.* prepared $LiFePO_4$ by a sol-gel process. It was found that the negative electrodes of aqueous lithium-ion batteries in a discharged state can react with water and oxygen, resulting in capacity fading upon cycling [19]. By eliminating oxygen and adjusting the pH values of the electrolyte, the $LiTi_2(PO_4)_3/Li_2SO_4/LiFePO_4$ aqueous lithium-ion batteries exhibited excellent stability with capacity retention over 90% after 1000 cycles at a current rate of 6 C and 85% after 50 cycles even at a low current rate of 1/8 C in pH=13 aqueous electrolyte. The electrochemical performance of

*Authors to whom correspondence should be addressed. E-mail: wen_yuehua@126.com, luyonglai@mail.buct.edu.cn, FAX: +86-10-64433964

 ©2015 Chinese Physical Society

commercial $LiFePO_4$ was determined by our group. It was found that the discharge capacity of commercial $LiFePO_4$ is just around 120 mAh/g and the cycling performance is poor. Apparently, the electrochemical performance for this commercial $LiFePO_4$ are quite different from the $LiFePO_4$ prepared by Luo *et al.* in aqueous medium [12]. A clear understanding of the $LiFePO_4$ electrochemical performance change as a function of pH value and its quantitative evaluation in aqueous medium is essential for designing an aqueous-based electrochemical system.

In the present work, a systematic investigation into the effect of pH on the electrochemical performance and the mechanism for the capacity fading of commercial $LiFePO_4$ has been carried out by means of cyclic voltammogram, ac impedance, *ex situ* X-ray diffraction (XRD), and chemical analysis. Furthermore, the correlation of charge-discharge performance for the commercial $LiFePO_4$ with organic and aqueous media was discussed.

II. EXPERIMENTS

Commercial $LiFePO_4$ powder was obtained from Tianjin (Tianjin Stl Energy Technology Co., Ltd) and no further treatment was performed. The working electrode was fabricated by compressing a mixture of the active materials ($LiFePO_4$), the conductive material (acetylene black), and the binder (polytetrafluoroethylene, PTFE) in a weight ratio of active materials:carbon:PTFE=85:10:5 onto a stainless steel grid by hydraulic machine at 20 MPa. The electrodes were made into the form of square typically (1 cm×1 cm), and then dried at 100 °C for 1 h. The weight of active material is typically in the range of 3−5 mg for each electrode sample. Li_2SO_4 or $LiNO_3$ aqueous electrolyte solution was prepared by dissolving Li_2SO_4 or $LiNO_3$ powder in distilled water and then the pH was adjusted by H_2SO_4, HNO_3 or LiOH solutions.

Cyclic voltammograms were obtained by using a three-electrode cell, in which the active carbon and saturated calomel electrode (SCE, 0.242 V *vs.* NHE) were used as counter and reference electrodes, respectively, and then performed using an electrochemical working station of CHI608D (Chenhua, Shanghai). Galvanostatic cycling with potential Limitation was tested on a special-purpose cell test instruments (Land). Electrochemical impedance measurements (EIM) were carried out with a Solarton instrument Model 1287 electrochemical interface, and the amplitude of the AC perturbation was 5 mV, the frequency range was 20 kHz to 0.1 Hz. All the measurements in aqueous electrolytes were made in a beaker cell. XRD measurements were performed on the electrode layers using a Panalytical X'Pert diffractometer with Cu Kα-radiation.

CVs of $LiFePO_4$ in organic electrolyte were carried out in the same way. The cells were prepared with Li metal foil as reference and counter electrodes, and 1 mol/L $LiPF_6$-EC/EMC/DMC (1/1/1, volume ratio) was used as the electrolyte solution. Celgard 2400 was used as the separator. Assembling of the cell was carried out in a glove box filled with argon gas. All electrochemical measurements were performed at ambient temperature.

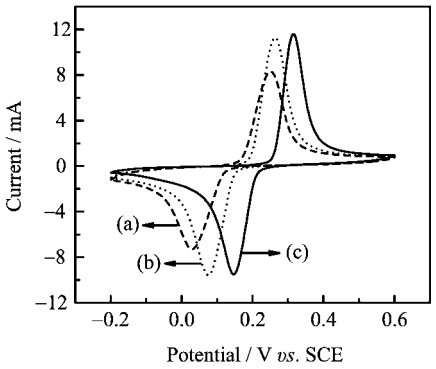

FIG. 1 Cyclic voltammograms of $LiFePO_4$ electrode at a scan rate of 1 mV/s in different aqueous electrolyte at pH=7. (a) 1 mol/L Li_2SO_4, (b) 2 mol/L $LiNO_3$, and (c) 5 mol/L $LiNO_3$.

III. RESULTS AND DISCUSSION

A. Effects of electrolytes and pH values

Figure 1 shows a typical cyclic voltammograms (CV) of $LiFePO_4$ electrode in different aqueous electrolyte of pH=7. These scans were initiated at −200 mV going in the anodic direction to +600 mV *vs.* SCE, respectively, which are in the safe potential window without O_2 and H_2 evolution [12] and then reversing the scan back to the starting potential. One pair of redox peaks are observed for $LiFePO_4$ tested under all aqueous electrolyte conditions, which agrees with the lithium-ion intercalation/de-intercalation process in an organic electrolyte. However, there are differences when the aqueous electrolyte or Li^+ concentration change. $LiFePO_4$ has higher oxidation and cathodic peak current in $LiNO_3$ solutions than that in Li_2SO_4 solutions with the same Li^+ concentration and pH value. It suggests that the polarization resistance of $LiFePO_4$ in $LiNO_3$ solutions is much smaller than that in Li_2SO_4 solutions as shown in Fig.1. The oxidation peak shifts to a high-potential position and the peak currents also increase obviously in 5 mol/L $LiNO_3$ solution due to the increase in the concentration of Li^+ ion. It is shown that the excellent kinetics and the higher electrode potential of $LiFePO_4$ can be obtained in an aqueous solution of 5 mol/L $LiNO_3$.

The dependence of the electrochemical stability of $LiFePO_4$ on the pH values of electrolyte was examined

DOI:10.1063/1674-0068/28/cjcp1502020 ©2015 Chinese Physical Society

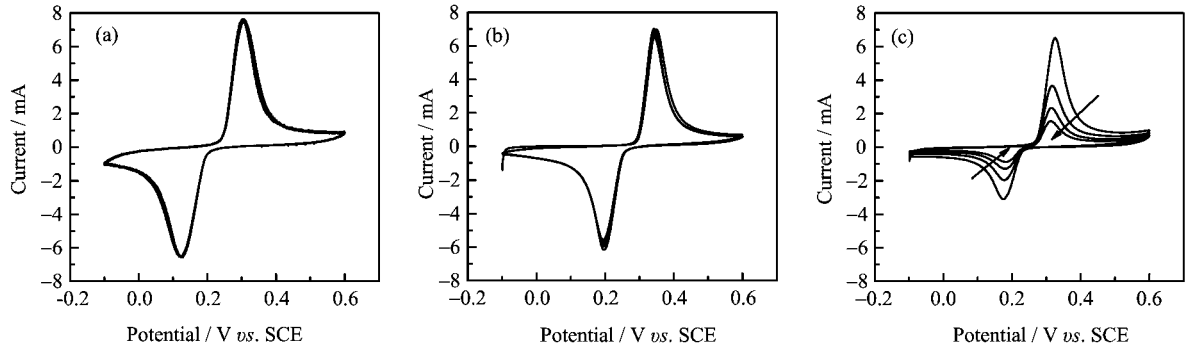

FIG. 2 Cyclic voltammograms of $LiFePO_4$ at the 1st, 2nd, 3rd, 4th and 5th cycles in 5 mol/L $LiNO_3$ solutions with various pH values. (a) pH=4, (b) pH=7, (c) pH=11.

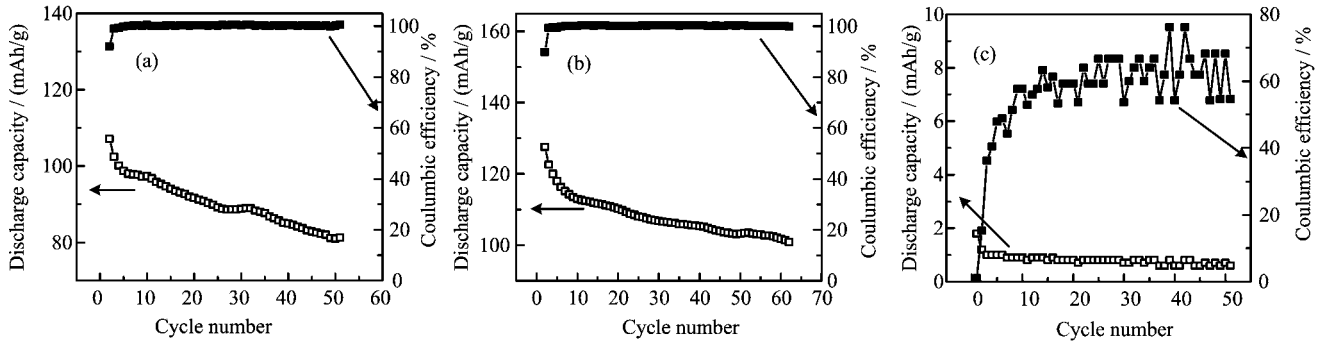

FIG. 3 Cycling behavior of the $LiFePO_4$ electrode at a rate of 1 C in 5 mol/L $LiNO_3$ with various pH values. (a) pH=4, (b) pH=7, (c) pH=11.

in 5 mol/L $LiNO_3$ solution of pH varying from 4 to 11. Cyclic voltammograms of $LiFePO_4$ in 5 mol/L $LiNO_3$ solutions with various pH values are shown in Fig.2. As can be seen, fast capacity fading upon cycling is detected only in 5 mol/L $LiNO_3$ aqueous solution of pH=11, while in both pH=4 and 7 aqueous solutions, $LiFePO_4$ undergoes a different process. The good overlap of the anodic and cathodic peaks in the subsequent cycles indicates that the $LiFePO_4$ electrode is relatively stable in $LiNO_3$ aqueous solutions of pH=4 or 7. This result does not agree with that reported by Luo *et al.* [12]. $LiFePO_4$ can be used over a pH range from 7 to 14 in aqueous solutions [12]. However, Yu *et al.* found that $LiFePO_4$ decomposed in a strong alkaline solution and the decomposition can be slowed down by carbon coating the material [16]. After prolonged storage in water, the specific capacity of carbon-coated $LiFePO_4$ is reduced and Fe dissolution is observed.

To find the reason of difference in the electrochemical performance of $LiFePO_4$ in aqueous solutions of various pH values, $LiFePO_4$ was cycled between 0 and 0.5 V *vs.* SCE at the rate of 1 C for 50 cycles in 5 mol/L $LiNO_3$ solutions of pH=4, 7, and 11, respectively, as shown in Fig.3. As can be seen, a sudden drop of the discharge capacity occurs during initial cycling in both pH=4 and 7 aqueous solutions just like the VO_2 in $LiNO_3$ aqueous electrolyte [9] and $LiTi_2(PO_4)_3/LiFePO_4$ in Li_2SO_4 aqueous electrolyte [12]. Subsequently, a slow decrease in the discharge capacity is exhibited during cycling. After 50 cycles, it still presents a discharge capacity of 80 and 100 mAh/g in 5 mol/L $LiNO_3$ of pH=4 and 7, exhibiting a relatively good cycling stability, especially in 5 mol/L $LiNO_3$ of pH=7. On the contrary, in solution of pH=11, the $LiFePO_4$ electrode cannot charge-discharge normally. Almost no discharge capacity is presented and the coulombic efficiency is lower than 80%. This may be caused by a lower zeta-potential of $LiFePO_4$ paste at pH=7 caused by an increased number of acid groups and a decreased number of basic groups [18]. To explain the above phenomenon, the Fe-content in 5 mol/L $LiNO_3$ aqueous solutions of different pH after 50 cycles was examined using the inductive coupled plasma emission (ICP) analysis. After 50 cycles, the content of Fe in the aqueous electrolyte of pH=7 is the lowest (only 0.04 ppm), the next is in the solution of pH=4 (0.19 ppm). The content of Fe in the solution of pH=11 is the highest (0.295 ppm). It is proven that the Fe dissolution of $LiFePO_4$ may be responsible for the poor cycling stability of $LiFePO_4$ in the aqueous solution of pH=11. Then the structure changes of $LiFePO_4$ before and after 50 cycles were analyzed by XRD.

The typical *ex situ* XRD patterns of $LiFePO_4$ before

DOI:10.1063/1674-0068/28/cjcp1502020 ©2015 Chinese Physical Society

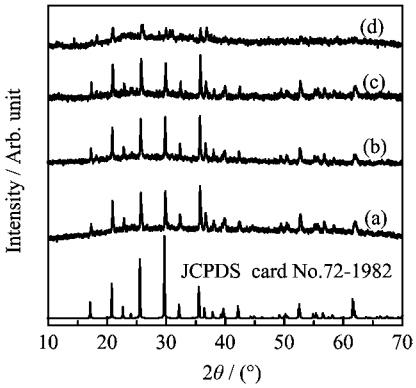

FIG. 4 *Ex situ* XRD patterns of $LiFePO_4$ electrode at different conditions. (a) Before cycling, (b) after cycling in pH=7 $LiNO_3$ solution, (c) after cycling in pH=4 $LiNO_3$ solution, (d) after cycling in pH=11 $LiNO_3$ solution.

cycling (before charge-discharge test, $LiFePO_4$ was at OCV state (0 V *vs.* SCE)) and after cycling (with 50 charge-discharge cycles, then $LiFePO_4$ was discharged to 0 V *vs.* SCE) in aqueous solutions of various pH values are given in Fig.4. The XRD pattern of the compound after cycling (Fig.4 (b) and (c)) is similar to that before cycling (Fig.4(a)), but all Brag diffraction peaks shift to the large angle, suggesting that a compound with a small lattice parameter is formed. In addition, only small and weak peaks of impurities appear. However, in solution of pH=11, Brag diffraction peaks become very weak at 2θ lower than 36°, while all diffraction peaks disappear at 2θ higher than 40°. This result agrees with that of the Fe dissolution determination of $LiFePO_4$.

B. Charge-discharge performance of $LiFePO_4$ electrodes

The rate capability of the $LiFePO_4$ was examined by applying different current densities during five cycles in organic electrolyte and aqueous electrolyte (see Fig.5). It indicated that the $LiFePO_4$ in organic electrolyte maintained good rate capability with initial discharge capacities of 166 mAh/g at 0.2 C, 157 mAh/g at 1 C, and 117 mAh/g at 4 C, respectively. By comparison, the $LiFePO_4$ in aqueous electrolyte exhibits the low initial discharge capacity of 105 mAh/g and poor rate capability with the discharge capacities of 70 mAh/g at 1 C, and only 50 mAh/g at 4 C. Poor electrochemical performance may be caused by the big particle size, both particle size minimization and intimate carbon contact are necessary to optimize electrochemical performance [19].

The cycling performances of the $LiFePO_4$ in organic electrolyte and in aqueous electrolyte are shown in Fig.6. It clearly shows that the capacity of the $LiFePO_4$ in aqueous electrolyte decreases faster, especially during the early cycles. At the same time, a lower initial capacity was found in this case. On the contrary, the $LiFePO_4$ in organic electrolyte exhibited improved capacity retention almost without capacity fading. The reversible capacity of the $LiFePO_4$ was approximately 140 mAh/g at 1 C in the case of using organic electrolyte.

To understand the electrolyte effect and the capacity fading mechanism of $LiFePO_4$ in aqueous electrolyte solutions, the diffusion coefficients of $LiFePO_4$ in $LiNO_3$

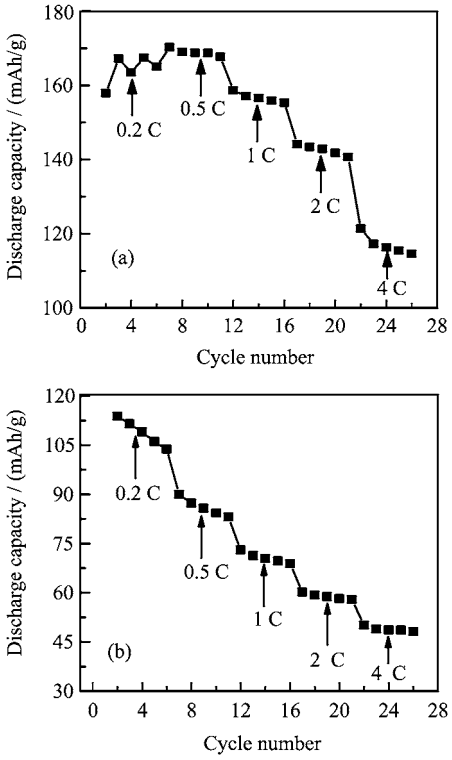

FIG. 5 The rate capability of $LiFePO_4$ at different current densities in (a) organic electrolyte and (b) 5 mol/L $LiNO_3$ aqueous electrolyte of pH=7.

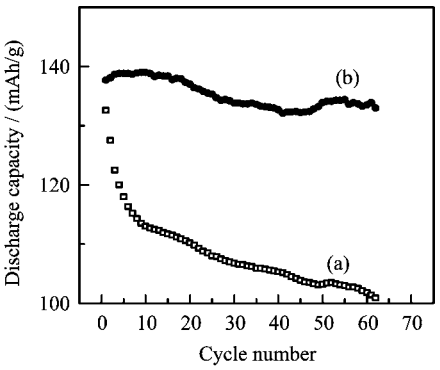

FIG. 6 Cycling performance of the $LiFePO_4$ at a rate of 1 C in (a) 5 mol/L $LiNO_3$ aqueous electrolyte of pH=7 and (b) organic electrolyte.

DOI:10.1063/1674-0068/28/cjcp1502020 ©2015 Chinese Physical Society

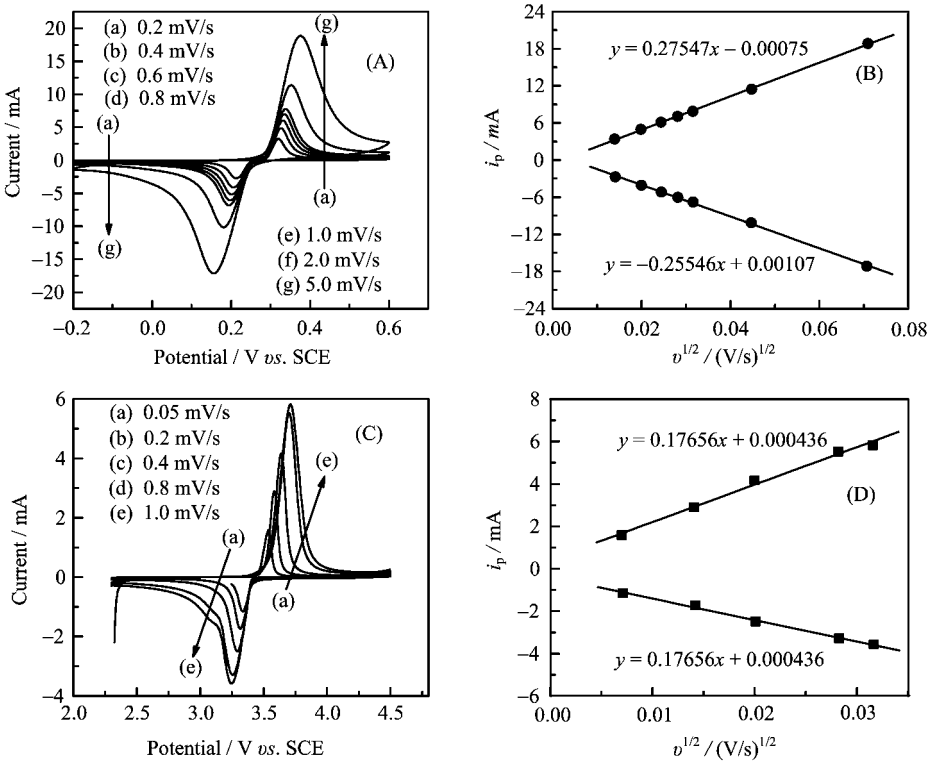

FIG. 7 The cyclic voltammograms of $LiFePO_4$ in $LiNO_3$ aqueous electrolyte (A) and organic electrolyte (C) with various scan rates. (B) and (D) show the anodic and cathodic peak current versus square root of scan rate for $LiFePO_4$ in aqueous $LiNO_3$ electrolyte and organic electrolyte.

aquous electrolyte and organic electrolyte were measured firstly. Figure 7 (B) and (D) show plots of the peak current densities *vs.* the square root of the potential sweep rate in organic electrolyte and aqueous electrolyte, respectively. For a mass transport controlled reaction, a linear increase of the peak current density with the square root of the potential sweep rate can be predicted by Randles-Sevcik equation [20–22]:

$$i_{\rm p} = 0.4463nF\sqrt{\frac{nF}{RT}}C\sqrt{v}A\sqrt{D} \qquad (1)$$

where $i_{\rm p}$ is the peak current and expressed in amperes, C is the concentration of lithium in mol/cm^3 (2.28×10^{-2} mol/cm^3), A is the surface area in cm^2, D is the diffusion coefficient of lithium through the solid phase in cm^2/s, and v is sweep rate in V/s. From the Randles-Sevcik plots, the diffusion coefficients were obtained and listed in Table I.

It can be seen that the diffusion coefficients for lithium extraction process is slightly higher than that for lithium insertion process in both aqueous and organic electrolyte. However, the average diffusion coefficient for lithium ions in aqueous electrolyte is higher almost one magnitude than that in organic electrolyte. It seems that the result is not consistent with the above electrochemical performance test. However, an experimental phenomenon is found, some white precipitate appeared on the surface of $LiFePO_4$ after long-term charge-discharge cycling. And then, it was dissolved by the HNO_3 solution and examined by the ICP analysis. The result shows that the precipitate is composed of Li, Fe and P with a mole ratio of Li:Fe:P=5:14:6. It is suggested that the formation of precipitate on the surface of $LiFePO_4$ may damage the crystalline structure of $LiFePO_4$ and leads to an increase in the lithium diffussion resistance. This change in crystalline structure can be confirmed from Fig.8 which is the *ex situ* XRD patterns of $LiFePO_4$ electrodes at pH=7 $LiNO_3$ and organic electrolyte after 70 cycles. It is observed that the XRD pattern of the compound after cycling in organic electrolyte (Fig.8(b)) is similar to the standard pattern of $LiFePO_4$. While, in the case of the XRD pattern of the compound after cycling in $LiNO_3$ electrolyte (Fig.8(a)), some Brag diffraction peaks turn to be ambiguous and peaks of impurities appear. These impurities peaks may be caused by the precipitate on the surface of $LiFePO_4$.

C. Electrochemical impedance spectra at different charge-discharge states

After one charge-discharge cycle at the current rate of 0.1 C to activate the $LiFePO_4$ electrode and then 1 cycle

DOI:10.1063/1674-0068/28/cjcp1502020 ©2015 Chinese Physical Society

TABLE I The diffusion coefficients of $LiFePO_4$ in $LiNO_3$ aquous electrolyte and organic electrolyte calculated from Randles-Sevcik equation.

	Diffusion coefficient/(cm^2/s)	
	Anodic	Cathodic
Aqueous	2.020×10^{-9}	1.735×10^{-9}
Organic	8.287×10^{-10}	2.742×10^{-10}

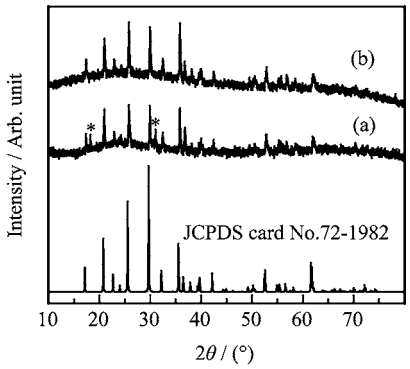

FIG. 8 *Ex situ* XRD patterns of $LiFePO_4$ electrode at (a) pH=7 $LiNO_3$ and (b) organic electrolyte after 70 cycles at a current rate of 1 C (the marks * are the peaks of impurities compared with the standard pattern of $LiFePO_4$).

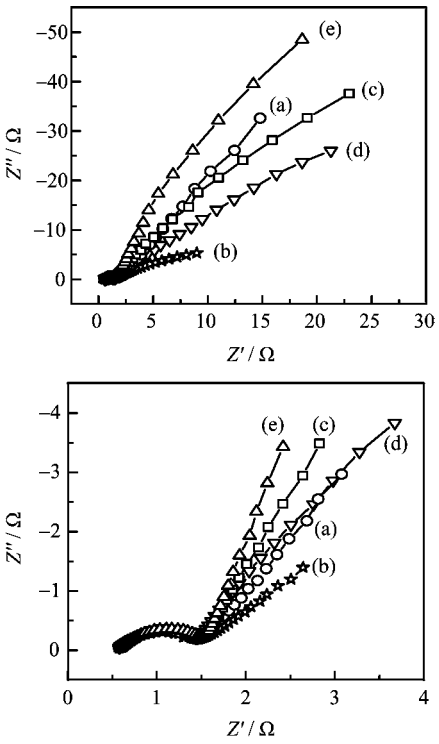

FIG. 9 AC impedance spectra of $LiFePO_4$ electrode at different states of 3rd charge/discharge cycle (1 C) in pH=7 $LiNO_3$ solution: (a) at the end of the 2nd cycle or the start of the 3rd cycle (0 V *vs.* SCE), (b) at the charge state (0.3 V *vs.* SCE) of the 3rd cycle, (c) at the nearly full charged state of the 3rd cycle (0.5 V *vs.* SCE), (d) at the discharge state of the 3rd cycle (0.16 V *vs.* SCE), and (e) at the end of the 3rd cycle (0 V *vs.* SCE).

at the current rate of 1 C to ensure the charge/discharge efficiency is close to 100% (99.8% here), we applied the AC impedance technique to monitor changes in aqueous electrolyte/$LiFePO_4$ interface resistance at different charge/discharge states of the 3rd cycle. Figure 9 gives the typical impedance spectra at different charge/discharge states of the 3rd cycle in pH=7 $LiNO_3$ solution. The plots show a high-frequency small arc and a long slant in the middle and low-frequency regions. This indicates that the electrode process of $LiFePO_4$ is controlled by solid-state diffusion of lithium ion in aqueous medium. The resistance detected at the charge state (Fig.9(b)) in which the Li ion was extracted is the lowest. The resistance turns to be the highest at the nearly full charged state in which the Li ion was almost extracted. A decrease in the resistance is observed at the discharge state. And at the end of the 3rd charge-discharge cycle, the impedance spectra have a visible difference from that at the start of the 3rd cycle (Fig.9(a), 0 V *vs.* SCE, before charge).

In order to study the change in the AC spectra of $LiFePO_4$ during the charge/discharge process in detail, equivalent circuits were employed to analyze the impedance spectra data shown above. The equivalent circuit is given in Fig.10, and the fitting goodness between the experiments and calculation is also shown in Fig.10. For the $LiFePO_4$ in aqueous medium at the discharge state of the 3rd cycle (0.16 V *vs.* SCE), typically one dispersed semicircle within the frequency range 20^3−100 Hz was observed (see Fig.10). The dispersed semicircle may include two overlapped semicircles. The total impedance could be considered the solution impedance in the high frequency, which can be represented by a resistance R_1, in series with the impedance in the medium frequency contributed from the charge-transfer process, which can be characterized by $R_{2\ Li^+}$||CPE combination, where $R_{2\ Li^+}$ is charge-transfer resistance, and CPE can be considered the double-layer capacitance. The $R_{2\ Li^+}$ is then in series with the impedance resulting from the side reaction in which the faradic-current branch can also be represented as R_3||CPE combination. The equivalent circuit is given in Fig.10(b). In other charge-discharge states, the shape of the impedance spectra and their equivalent circuit are the same as that shown in Fig.10. The fitting results, including solution resistance R_1, lithium-ion intercalation charge-transfer resistance $R_{2\ Li^+}$, side reaction charge transfer R_3, and diffusion resistance W_1-R are summarized in Table II. As shown in Table II, with the change of the charge-discharge states the solution resistance R_1 almost keeps constant. While charge-

DOI:10.1063/1674-0068/28/cjcp1502020 ©2015 Chinese Physical Society

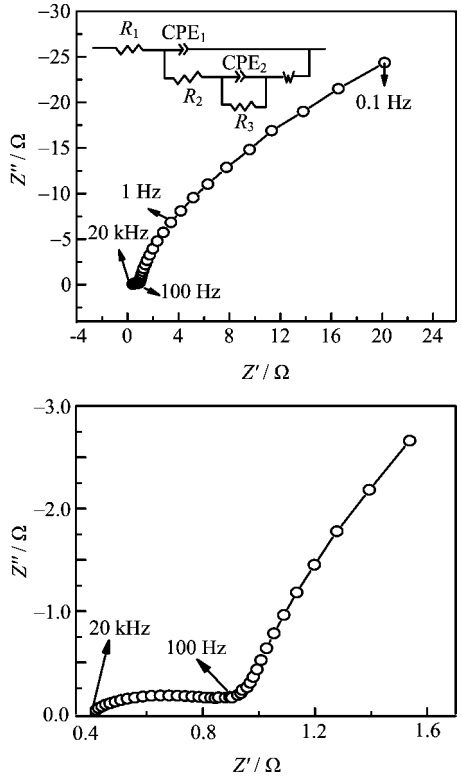

FIG. 10 AC impedance plots of $LiFePO_4$ electrode at the discharge state of the 3rd cycle (0.16 V *vs.* SCE) and its equivalent circuit (○ is the test result and line is the fitting result).

transfer resistance for lithium-ion $R_{2\ Li^+}$ and diffusion resistance W_1-R at the discharge states are larger than that at the charge states. It indicates that the lithium-ion intercalation is more difficult than the lithium-ion extraction. However, from the charge state to the discharge state, the charge transfer resistance for side reactions R_3 increased sharply. Furthermore, the increase of R_3 mainly occurs at the charge process. For example, at the charge state of 0.3 V *vs.* SCE, the R_3 is reduced to only 0.7 Ω. When this electrode is charged to 0.5 V *vs.* SCE, the R_3 increases to be 12 Ω, which is close to the R_3 at the discharge states of 0.16 and 0 V *vs.* SCE. This suggests that the side reactions mainly occur during the charge process, which should be ascribed to the Li loss and the formation of precipitate demonstrated by the above ICP analysis. At last, the R_3 at the discharge states of 0 V (curve (e), 0 V *vs.* SCE, after charge-discharge of the 3rd cycle) is 10.04 Ω, which is bigger than that at the end of the 2nd cycle (5.7 Ω, curve (a), 0 V *vs.* SCE, after charge-discharge of the 2nd cycle). This may be one reason for the fast decrease of discharge capacity from cycle 2 to cycle 3 (see Fig.6(a)).

TABLE II Summaries of the fitting results of solution resistances (R_1), charge-transfer resistances for Li^+ (R_2), resistances for the side reaction (R_3) and diffusion resistances (W_1-R) at different charge/discharge state of the 3rd cycle.

State	R_1/Ω	R_2/Ω	R_3/Ω	W_1-R/Ω
Start at 0 V	0.37961	0.36827	5.7	0.61
Charge at 0.3 V	0.38795	0.35987	0.70	0.53
Charge at 0.5 V	0.38904	0.36841	11.88	0.53
Discharge at 0.16 V	0.39248	0.40602	14.92	0.59
Discharge at 0 V	0.39199	0.40250	10.04	0.65

IV. CONCLUSION

In this work, it is found that $LiFePO_4$ has a relatively stable electrochemical performance in $LiNO_3$ aqueous solution with pH=7, and with the pH value increased to pH=11, a sharp decay in the electrochemical properties of $LiFePO_4$ is presented. Though the diffusion coefficient of lithium through the solid phase of $LiFePO_4$ in aqueous electrolyte is higher than that in organic medium, its electrochemical performance is inferior to that in organic electrolyte. It is attributed to a fact that during prolonged charge-discharge in aqueous medium, the loss of Li and Fe, P dissolution occurs, forming a precipitate on the surface of $LiFePO_4$ electrodes. It results in the change of crystalline structure, a large electrode polarization and the capacity fading of $LiFePO_4$.

V. ACKNOWLEDGMENTS

This work was supported by the Research Institute of Chemical Defence (Beijing, China).

[1] A. K. Padhi, K. S. Nanjundaswamy, and J. B. Goodenough, J. Electrochem. Soc. **144**, 1188 (1997).
[2] S. H. Ju and Y. C. Kang, Mater. Chem. Phys. **107**, 328 (2008).
[3] M. Yonemura, A. Yamada, Y. Takei, N. Sonoyama, and R. Kanno, J. Electrochem. Soc. **151**, A1352 (2004).
[4] A. Eftekhari, J. Electrochem. Soc. **151**, A1816 (2004).
[5] M. S. Whittingham, Y. Song, S. Lutta, P. Y. Zavalij, and N. A. Chernova, J. Mater. Chem. **15**, 3362 (2005).
[6] W. Li and W. R. McKinnon, J. Electrochem. Soc. **141**, 2310 (1994).
[7] W. Li and J. R. Dahn, J. Electrochem. Soc. **142**, 1742(1995)
[8] W. Li, J. R. Dahn, and D. S. Wainwright, Science **264**, 1115 (1994).
[9] M. J. Zhang and J. R. Dahn, J. Electrochem. Soc. **143**, 2730 (1996)
[10] M. S. Zhao, Q. Y. Zheng, F. Wang, W. M. Dai, and X. Song, Electrochimica Acta **56**, 3781 (2011).

DOI:10.1063/1674-0068/28/cjcp1502020 ©2015 Chinese Physical Society

[11] J. Kohler, H. Makihara, H. Uegaito, H. Inoue, and M. Toki, Electrochimica Acta **46**, 59 (2000).
[12] J. Y. Luo, W. J. Cui, P. He, and Y. Y. Xia, Nat. Chem. **2**, 760 (2010).
[13] H. B. Wang, K. L. Huang, Y. Q. Zeng, S. Yang, and L. Q. Chen, Electrochimica Acta **52**, 3280 (2007).
[14] J. Y. Luo and Y. Y. Xia, Adv. Funct. Mater. **17**, 3877 (2007).
[15] W. Porcher, P. Moreau, B. Lestriez, S. Jouanneau, and D. Guyomard, Electrochem. Solid-State Lett. **11**, A4 (2008)
[16] D. Y. Yu, K. Donoue, T. Kadohata, T. Murata, S. Matsuta, and S. Fujitani, J. Electrochem. Soc. **155**, A526 (2008).
[17] J. F. Martin, A. Yamada, G. Kobayashi, S. Nishimura, S. Kanno, D. Guyomard, and N. Dupreé, Electrochem. Solid-State Lett. **11**, A12 (2008).
[18] J. H. Lee, H. H. Kim, G. S. Kim, D. S. Zang, Y. M. Choi, H. Kim, D. K. Yi, W. M. Sigmund, and U. Paik, J. Phys. Chem. C **114**, 4466 (2010).
[19] H. Huang, S. C. Yin, and L. F. Nazar, Electrochem. Solid-State Lett. **4**, A170 (2001).
[20] V. Srinivasan and J. Newman, J. Electrochem. Soc. **151**, A1517 (2004).
[21] K. Wang, R. Cai, T. Yuan, X. Yu, R. Ran, and Z.P. Shao, Electrochimica Acta **54**, 2861 (2009).
[22] W. L. Liu, J. P. Tu, Y. Q. Qiao, J. P. Zhou, S. J. Shi, X. L. Wang, and C. D. Gu, J. Power Sources **196**, 7728 (2011).

DOI:10.1063/1674-0068/28/cjcp1502020 ©2015 Chinese Physical Society